Nanoscale

# Enhancing Circular Dichroism by Chiral Hotspots in Silicon Nanocube Dimers



| | |
|---|---|
| Journal: | *Nanoscale* |
| Manuscript ID | NR-ART-01-2018-000902.R1 |
| Article Type: | Paper |
| Date Submitted by the Author: | 18-Mar-2018 |
| Complete List of Authors: | Yao, Kan; Northeastern University<br>Liu, Yongmin; Northeastern University, Department of Mechanical & Industrial Engineering, Department of Electrical & Computer Engineering |
| | |

Nanoscale

ARTICLE

# Enhancing Circular Dichroism by Chiral Hotspots in Silicon Nanocube Dimers

Received 00th January 20xx,
Accepted 00th January 20xx

DOI: 10.1039/x0xx00000x

www.rsc.org/

Kan Yao[a] and Yongmin Liu[a,b,†]

Circular dichroism (CD) spectroscopy, which measures the differential absorption of circularly polarized light with opposite handedness, is an important technique to detect and identify chiral molecules in chemistry, biology and life sciences. However, CD signals are normally very small due to the intrinsically weak chirality of molecules. Here we theoretically investigate the generation of chiral hotspots in silicon nanocube dimers for CD enhancement. Up to 15-fold enhancement of the global optical chirality is obtained in the dimer gap, which boosts the CD signal for one order of magnitude without reducing the dissymmetry factor. The origin of this chiral hotspot arises from the simultaneous enhancement of magnetic and electric fields and their proper spatial overlap. Our findings could lead to integrated devices for CD spectroscopy, enantioselective sensing, sorting and synthesis.

## 1. Introduction

An object is chiral if it is not superimposable to its mirror image. The existence of chirality in nature is universal, ranging from bulky galaxies spanning some thousands light years to gastropod shells with size in a few centimeters and to molecules at the nanoscale. While a pair of chiral molecules, termed as enantiomers, share the same scalar physical properties, they could function differently in biological and chemical processes, acting in a desirable or harmful way. Therefore, discriminating between enantiomers is of vital importance, especially in pharmacology and life sciences.

Light can be chiral as well. Circularly polarized light (CPL) with opposite handedness has its electric and magnetic field vectors rotating clockwise or counterclockwise during propagation. Because chiral objects interact with CPL differently, chiral light-matter interactions provide an opportunity to noninvasively identify chiral molecules with superior precision. For example, circular dichroism (CD) spectroscopy that measures the differential absorption of left- and right-circularly polarized (LCP/RCP) light is widely used to investigate the structural information of chiral molecules.[1] However, CD signals are usually very weak due to the intrinsically weak chirality of the target molecules. In order to enhance CD signals for low-concentration or even single molecule detection, various approaches have been proposed by utilizing standing waves,[2,3] plasmonic resonances,[4-12] magnetic resonances,[13,14] and nano-cavity resonators,[15] etc.[16] Despite improved differential absorption by the chiral molecules, these methods suffer from either strong background absorption by the nanostructures or non-uniform chiral fields that hinder the global CD enhancement. Both issues impose significant limitations on the achievable measurement sensitivity. Therefore, new platforms exhibiting low loss and uniform superchiral fields are highly desirable.

In this work, we theoretically investigate a new scheme to generate chiral hotspots in achiral silicon nanocube dimers for CD enhancement. High-refractive-index dielectric nanoparticle dimers have been used to enhance electric or magnetic field in the gap region under the excitation of linearly polarized light (LPL) at visible wavelengths.[17] By changing the illumination to CPL, the localized electric and magnetic fields are simultaneously enhanced. As a result, the spatially overlapped electric and magnetic hotspots can result in a uniform chiral hotspot with maximized chirality density when an appropriate phase condition is satisfied. With our proposed silicon nanocube dimers, a volume-averaged chirality enhancement of up to 15-fold is demonstrated by simulations, which amplifies the CD signal for over one order of magnitude. Because the dimer is achiral and the loss of silicon is low (thanks to the indirect bandgap of silicon) in the visible region, very weak background absorption is present, which promises a moderately high dissymmetry factor. Our design generates strong and uniform chiral fields without employing complex architectures or plasmonic materials. We foresee that our work could inspire novel devices, especially on-chip photonic components for (surface-enhanced) CD spectroscopy, enantioselective sensing, sorting, synthesis, and photolysis.

[a] Department of Electrical and Computer Engineering, Northeastern University, Boston, Massachusetts 02115, USA.
[b] Department of Mechanical and Industrial Engineering, Northeastern University, Boston, Massachusetts 02115, USA.
† Corresponding Author: y.liu@northeastern.edu
Electronic Supplementary Information (ESI) available: (I) Dependence of chirality on the dimer's geometric parameters; (II) Influence of the native oxide layer on chirality enhancement; (III) Modeling of chiral molecules as a bulk medium. See DOI: 10.1039/x0xx00000x

## 2. Optical chirality and dissymmetry factor

The chirality of an optical field can be characterized by the optical chirality density *C*. The definition of *C*

$$C \equiv \frac{\varepsilon_0}{2} E \cdot \nabla \times E + \frac{1}{2\mu_0} B \cdot \nabla \times B = -\frac{\omega \varepsilon_0}{2} \mathrm{Im}(\mathbf{E}^* \cdot \mathbf{B}) \quad (1)$$

was first introduced by Lipkin[18] while the physical significance of this quantity was revealed by Tang and Cohen.[2,3] In Equation (1), $E$ ($\mathbf{E}$) and $B$ ($\mathbf{B}$) represent the real (complex) electric and magnetic vector fields respectively, and $\varepsilon_0$ and $\mu_0$ are the permittivity and permeability of vacuum, respectively. For CPL in free space, the chirality $C_0 = \pm\omega\varepsilon_0|E|^2/(2c)$, where $c$ is the speed of light in the vacuum and the plus/minus sign corresponds to right/left handedness. By utilizing nanostructures, it is possible to generate CPL-induced near fields exhibiting local chirality density greater than $C_0$, which can significantly enhance the interaction between light and chiral matter. When a chiral molecule, described by complex-valued electric polarizability $\alpha$, magnetic susceptibility $\chi$, and chiral (or mixed) polarizability $G$, interacts with a chiral field, its absorption can be expressed by:[19]

$$A^{\pm} = \frac{\omega}{2}(\alpha''|\mathbf{E}|^2 + \chi''|\mathbf{B}|^2) \mp \frac{2}{\varepsilon_0} G''|C| \quad (2)$$

with $A^+/A^-$ being the absorption rate under LCP/RCP excitation and superscripts '' denoting the imaginary part of the corresponding molecular quantities. Note that the third term on the right side has a sign determined by the handedness of the incident field. Therefore, the differential absorption induced by a chiral molecule is:

$$\Delta A = A^+ - A^- = -\frac{4}{\varepsilon_0} G''|C|, \quad (3)$$

and the associated CD signal is proportional to $\Delta A$. Obviously, the enhancement of chirality $C$ will amplify the CD signal from a chiral molecule by a factor of $C/C_0$.

Another important quantity in enantioselective sensing and synthesis is the dissymmetry factor $g$. Taking the ratio of CD to the sum of the absorption subject to LCP and RCP illumination, we can define the dissymmetry factor

$$g = \frac{2(A^+ - A^-)}{A^+ + A^-}. \quad (4)$$

It characterizes the chiral asymmetry of a molecule in the absorption rate. The physical significance of $g$ is that it gives a criterion of whether or not the CD in a certain absorption band is measureable.[19] More importantly, $g$ sets the limit of the efficiency of enantioselective photochemical reactions, which is critical for efficient separation of racemic mixtures. Provided that the second term in Equation (2) involving $\chi''$ is always negligibly small in the optical region, Equation (4) reduces to

$$g = -\frac{8}{\omega\varepsilon_0}\frac{G''}{\alpha''}\frac{|C|}{|\mathbf{E}|^2}. \quad (5)$$

Unlike the chirality density $C$ in Equation (1) that can be enhanced by boosting either the electric or magnetic field and by engineering their relative phase, the $g$-factor favors larger $C$ yet a less intense electric field. To this end, enhancing the magnetic component of an optical chiral field is the optimal strategy to facilitate the enhancement of both CD and $g$-factor.

In practice, however, it is very difficult to enhance the magnetic field alone. Plasmonic nanostructures can increase the local electric field intensity significantly, while the modification of magnetic field intensity is weak and the magnetic hotspots are often inaccessible. High-refractive-index dielectric nanoparticles can support Mie resonances, in particular magnetic resonances at optical wavelengths, offering a unique alternative to generate magnetic hotspots where the enhancement of local magnetic field intensity is comparable to that of the electric field.[17,20] In addition, the low-loss property and compatibility with semiconductor fabrication processes also make high-index dielectrics very attractive for advanced photonic devices. Unfortunately, individual dielectric particles do not support resonant modes that can globally maximize the chirality density $C$.[13,14] Therefore, we need to seek pragmatically engineered nanostructures to obtain strong and uniform chiral fields with simultaneously enhanced optical chirality density and dissymmetry factor.

## 3. Chiral hotspots in silicon nanocube dimers

We consider a silicon nanocube dimer immersed in a matrix medium with refractive index $n$ = 1.33, given that chiral molecules are dispersed in solution as in most experiments. This choice of index is also reasonable when the dimer is fabricated on a low-index substrate such as quartz and magnesium fluoride, mimicking the scenario of surface-enhanced CD measurements.[10,11,13] High-refractive-index dielectric nanoparticles have aroused broad interest for photonic applications because they support strong magnetic resonances at visible wavelengths in addition to electric resonances. When resonant particles are placed in close proximity, their coupling produces polarization-dependent hotspots.[17] Figure 1(a) and (b) illustrate two representative configurations for a silicon nanocube dimer: When the incident electric field is polarized parallel to the dimer axis, an electric hotspot (red) occurs in the gap due the excitation of electric dipoles (p); alternatively, when the incident magnetic field is polarized parallel to the dimer axis, a magnetic hotspot (blue) arises due to the excitation of magnetic dipoles (m). In both cases, the hotspot is not chiral because of symmetry. However, for CPL incidence, the hotspot could be strongly chiral due to the superposition of the two linear polarization states, as sketched in Figure 1(c).

In our design, the edge length of the nanocubes is chosen to be 100 nm, and the gap size is 10 nm. Both are consistent with the state-of-the-art electron-beam lithography and focused ion beam milling techniques.[21] To account for the roundedness of the edges and corners that very likely exist in realistic structures, a local radius of 15 nm is used in modeling the nanocubes by finite-element electromagnetic solver COMSOL Multiphysics. We set the origin of the coordinate system at the inversion center of the dimer (note that the structure is centrosymmetric), and the dimer axis is along the

*y*-axis. The dielectric property of silicon is taken from Palik.[22] The black curve in Figure 2(a) shows the spectrum of the optical chirality averaged over the dimer gap region (70 nm × 70 nm × 10 nm) for RCP illumination (propagating along -*z*-axis), which is normalized to the optical chirality of CPL in the matrix medium without the presence of nanocubes. There is an evident broad peak centered at 555 nm with an over 15-fold enhancement factor. In Figure 2(a), we also plot the spectra of absorption (blue), scattering (red) and extinction (green). It can be identified that the peak of the scattering spectra at 550 nm corresponds to a magnetic resonance, while the peak at 470 nm corresponds to an electric resonance (see the following discussion on Figure 3). Due to the finite quality factor, the two resonances still have a spectral overlap, giving rise to the chirality enhancement maximum around 555 nm. To map the spatial distribution of the local chirality density, in Figure 2(b) we shows the field profile on a two-dimensional (2D) cross-sectional view in the mirror symmetry plane that is perpendicular to the dimer axis (*i.e.* the *y*=0 plane). A chiral hotspot is clearly seen at the gap center, exhibiting a maximum enhancement factor of 22. Within this cutting plane, the amplitude of the enhancement factor decreases gradually from the center while the sign maintains to be the same as for the incident CPL. In other words, because the structure is achiral, when the handedness of the incident light is reversed, an identical distribution of chirality in the opposite sign can be obtained. From a practical point of view, only the chiral molecules adsorbed on the dimer can interact with the local field efficiently, as the field intensity decays quickly from the vicinity of the resonant particles into the surrounding medium. We thus further examine the chirality enhancement at all the surfaces of the nanocubes. The results are presented in Figure 2(c) and (d). It can be seen that over the entire structure the surface chirality density has the same sign. Moreover, strong optical chirality appears only on the two facets forming the gap, and the distribution is similar to the previous map at the gap center. This confirms that the chiral hotspot in the dimer gap is fairly uniform, providing an excellent platform to enhance CD signals once molecules are adsorbed onto the dimer. Here we remark that the maximum intensity of the chiral hotspot is mainly correlated with the gap size, while the resonance wavelength is more sensitive to the cube's size and shape (see Figures S1 and S2 in the Electronic Supplementary Information). The native oxide layer that is very likely to occur under ambient conditions will diminish the enhancement factor slightly and cause blue-shift of the resonances (see Figure S3).[23]

The origin of the chiral hotspot is further explored from a microscopic view. Figure 3(a) and (b) show respectively the snapshots of magnetic and electric fields at 550 nm on the *y*=0 plane. In accord with the spectra in Figure 2(a), a magnetic hotspot is evidenced at the gap center in Figure 3(a). The magnitude peaks at the center with an enhancement factor of about 6, similar to the value reported in Ref. 15, maintains fairly uniform in the gap along the dimer axis (data not shown) and decreases in the lateral (*x*- and *z*-) direction. On the other hand, although the electric mode is not on resonance at 550 nm, Figure 3(b) shows a comparable enhancement of electric field with two maxima at the bottom and top edges of the gap. This hourglass-like pattern is complementary to the profile in Figure 3(a), indicating that the product of electric and magnetic fields will be relatively uniform. According to the definition in Equation (1), optical chirality is maximized when the electric and magnetic fields are parallel and have a $\pi/2$ phase difference. Figure 3(c) depicts the relative phase between $E_y$ and $B_y$, which are dominant among all the six components of the vectorial fields. One can see that the relative phase is indeed $\pi/2$ at the gap center, satisfying the required phase condition for optical chirality enhancement. Recalling that the parallel components of the electric and magnetic fields in CPL have an intrinsic $\pi/2$ phase difference, we could remark that the silicon dimer "squeezes" CPL to the gap by enhancing equally the amplitude of the constituent fields but not disturbing their phase relation. As shown in the 2D map in Figure 3(c), the phase varies linearly in the propagation direction but does not deviate much ($<\pi/6$) from the ideal value. Therefore, we can conclude that it is the simultaneous enhancement of magnetic and electric fields and their proper spatial overlap giving rise to the chiral hotspot in the dimer gap.

## 4. Enhancing CD by chiral hotspots

The chiroptical properties of a medium composed of randomly oriented chiral molecules are characterized by its relative electric permittivity $\varepsilon_r$, relative magnetic permeability $\mu_r$, and Pasteur parameter $\kappa$ describing the chiral response. The constitutive relations of Maxwell's equations, accordingly, are written in the following form:[24]

$$\mathbf{D} = \varepsilon_0\varepsilon_r\mathbf{E} + \mathrm{i}\kappa\mathbf{H}/c, \qquad (6a)$$

$$\mathbf{B} = \mu_0\mu_r\mathbf{H} - \mathrm{i}\kappa\mathbf{E}/c. \qquad (6b)$$

Here, assuming the chiral medium is isotropic, both $\varepsilon_r$ and $\kappa$ are frequency-dependent, complex-valued functions in general, while $\mu_r$ = 1. Based on the conclusion from Equation (3) drawn for a single molecule, the CD signal of a chiral medium should be proportional to the optical chirality $C$ and the imaginary part of the Pasteur parameter $\kappa$.

The modeling of chiral media relies on proper formalism of the material properties, especially the chiral parameter $\kappa$. Here, we adopt the convenient expressions derived by Govorov and coworkers:[25,26]

$$\varepsilon_r = \varepsilon_{r0} - \gamma\left(\frac{1}{\hbar\omega-\hbar\omega_0+\mathrm{i}\Gamma} - \frac{1}{\hbar\omega+\hbar\omega_0+\mathrm{i}\Gamma}\right), \qquad (7)$$

$$\kappa = \beta\left(\frac{1}{\hbar\omega-\hbar\omega_0+\mathrm{i}\Gamma} + \frac{1}{\hbar\omega+\hbar\omega_0+\mathrm{i}\Gamma}\right), \qquad (8)$$

where $\omega_0 = 2\pi c/\lambda_0$ with $\lambda_0$ the molecular resonance wavelength, $\Gamma$ is the resonance broadening, $\gamma$ and $\beta$ are coefficients related to the optical dipole moments and molecular density. All these parameters can be calibrated from measured extinction and CD spectra (see Supplementary Information).

Enhanced CD signals are expected when the molecular resonance well overlaps the maximized optical chirality. Albeit ultraviolet light is more well-known for exciting electronic transitions associated with CD, a lot of biomolecules also show optical activities in the visible region. For instance, bacteriorhodpsin (bR) in purple membrane has a positive CD band centered at about 530 nm and a negative band at 600 nm, and their complex interplay leads to a negative couplet near 570 nm.[27] Here we consider chiral molecules that have a distinct positive CD band at 550 nm. Its spectroscopic properties are taken to be $\varepsilon_{\text{ext,max}}$ = 50000 $M^{-1}cm^{-1}$ for molecular extinction, $\Delta_{\text{FWHM}}$ = 98 nm for bandwidth, and $\varepsilon_{\text{CD,max}}$ = 20 $M^{-1}cm^{-1}$ for molecular CD, similar to those of the bR molecules. By further assuming $\varepsilon_{r0}$ = 1.5 and the molecular density $n_0$ = (7 Å)$^3$,[28,29] all the unknown coefficients in Equations (7) and (8) can be determined. The resultant values are $\Gamma$ = 0.2 eV, $\gamma$ = 1.03 eV, and $\beta$ = 7.78 × $10^{-5}$ eV. Figure 4(a) and (b) show the dispersion of the Pasteur parameter and permittivity, respectively. As can be seen, the amplitude of $\kappa$ is in the order of $10^{-4}$, indeed very small compared with the dielectric function, reflecting the fact that the chiral response of molecules is intrinsically weak.

To demonstrate CD enhancement by the chiral hotspots, a chiral medium nanoslab (70 nm × 70 nm × 10 nm) with material properties shown in Figure 4(a) and 4(b) is inserted into the dimer gap. In practical circumstances, molecules will be adsorbed on all the facets of the nanocubes instead of just filling the gap.[30] However, as shown in Figure 2(d), the electric, magnetic, and chiral hotspots are all located in the gap with their amplitude much greater than those on other surfaces. Therefore, the contribution from molecules in the gap will dominate the global CD signal, whereas other surfaces can be reasonably ignored. In addition, if *in-situ* measurement is not required, the molecules outside the gap can be removed by proper techniques such as etching,[31] resulting in the identical configuration as in our model. Figure 4(c) compares the CD signals based on absorption cross-section when the chiral slab is coupled with the nanocube dimer (red and blue curves) or stands alone (black curve and inset). For experiments in a bulk solution containing numerous dimer-molecule composites, they can be converted to molar absorption coefficients in the standard (cgs) units $M^{-1}cm^{-1}$.[25] Notice that due to the relatively high refractive index of the chiral medium and the finite size of the slab, the CD signal of bare molecules exhibits two peaks. The one near 530 nm corresponds to the intrinsic CD band of the molecules, whereas the other at 460 nm is induced by the resonance of the slab. When chiral molecules are adsorbed to the dimer gap, it is observed that the composite (chiral molecules and silicon dimer) shows a much stronger CD peak at 550 nm (red curve), which is in good agreement with the chirality spectrum. Moreover, if we separate the contributions from chiral molecules and the silicon dimer, the CD signal from molecular absorption (blue curve) is even greater. This is because when the chiral molecules absorb more LCP light than RCP light intrinsically, the local field is slightly less intense under LCP excitation. Consequently, the induced CD signal from dimer absorption has an opposite sign that partially cancels out the molecular CD. Based on these results, in Figure 4(d) we calculate the CD enhancement factor by normalizing the CD spectra of the composite to that of the bare chiral slab. As can be seen, the CD signal based on absorption (red and blue curves) is enhanced by a factor of 8. Compared with the chirality spectrum in Figure 2(a), the decreased enhancement factor is caused by the high index of the chiral medium, which disturbs the local field and diminishes the chirality density in the dimer gap when molecules are in presence. In Figure 4(d), the CD signal based on extinction (black curve) is also shown. Unlike bare molecules that have almost identical absorption and extinction, the composite with silicon nanocubes scatters chiral light differently. The differential scattering is significant throughout the spectrum and does not have a uniform sign. Therefore, the overall extinction shows a complex line shape, giving rise to multiple CD peaks.

For chiral molecules, the typical ranges of molar extinction and CD are in the order of $10^4$ and 10 $M^{-1}cm^{-1}$, respectively. To demonstrate the generality of using silicon dimers for CD enhancement, in Figure 5 we consider another molecule with $\varepsilon_{\text{ext,max}}$ = 10000 $M^{-1}cm^{-1}$ and $\varepsilon_{\text{CD,max}}$ = 10 $M^{-1}cm^{-1}$. Since the refractive index of this molecule is close to the background medium, the intrinsic CD in Figure 5(c) (black curve and inset) shows a single CD band, and the CD enhancement factor in Figure 5(d) (red and blue curves) well resembles the chirality spectrum in Figure 2(d), giving a factor of over 12.

Lastly, the distribution of normalized dissymmetry factor $g$ is shown in Figure 6(a). The highest value exceeds 1 and occurs at the gap center overlapping the chiral hotspot. According to the definitions in Equations (1) and (5), this again confirms that the local magnetic field is enhanced almost equally as the local electric field. In the exceptional case where a single chiral molecule is adsorbed to the gap center with its dipole moments along the dimer axis, not only the resulting CD signal will be amplified by a factor of over 20, the difference in its excitation rate will also be enlarged slightly, which potentially increases the likelihood to separate enantiomers in a racemic mixture by an optical means.[14,32-34] The volume-averaged value of dissymmetry factor, nevertheless, decreases to about 0.9, which agrees well with the value of 0.8 retrieved from Figure 5(c). Both are much higher than the achievable dissymmetry factor in plasmon-enhanced CD, in which case the local electric field makes the dominant contribution to the CD enhancement while diminishes the dissymmetry factor.

It has been previously shown that LPL can also excite enhanced optical chirality in the gap of metallic nanoparticle dimers.[8] The mechanism is based purely on plasmonic resonances, where the local electric field is enhanced and it has a $\pi/2$ phase delay compared with the incident field, while the magnetic field is not modified. In dielectric dimers, however, this is not the case. The magnetic resonance is Mie-type and the magnetic hotspot does not carry such a phase delay. As confirmed in Figure 3(c), the relative phase between electric and magnetic components of the incident CPL is preserved in the gap. Similarly, when the dimer is illuminated by LPL with its polarization oriented 45° with respect to the dimer axis, although the electric and magnetic hotspots can

still be excited simultaneously, they inherit near-zero relative phase from the incident field. Therefore, the phase condition of optical chirality is not fulfilled. In Figure 6(b), we compare the volume-averaged chirality by CPL and LPL. While the extinction spectra are identical (see Figure 2(a)), the chirality for LPL illumination almost vanishes at 550 nm and is relatively weak throughout the visible region. Further inspection reveals that with LPL, two weak chiral hotspots in opposite signs co-exist in the dimer gap, and their contributions in CD enhancement cancel out. In plasmonic dimers, the associated Ohmic loss causes strong background absorption in the particles and dramatically decreases the dissymmetry factor. In addition, the LPL excitation scenario requires alignment of the light polarization to the dimer axis. This limits the application to arrays of uniformly oriented dimers. To these regards, dielectric dimers can provide simultaneous enhancement of electric and magnetic fields under CPL excitation, and they are superior for chiral hotspots generation.

## 5. Conclusions

In conclusion, we have numerically studied the generation of chiral hotspots in achiral silicon nanocube dimers and demonstrated the associated benefit for CD enhancement. Taking advantage of the high refractive index of silicon, a uniform chiral hotspot can be excited in the dimer gap based on the interplay between a magnetic hotspot and an electric hotspot. This, to the best of our knowledge, is the first attempt to enhance optical chirality with both the electric and magnetic constituents. A volume-averaged enhancement factor of about 15-fold is obtained. When chiral molecules are adsorbed in the gap area, the CD signal is enhanced for over one order of magnitude, which agrees well with the chirality enhancement. Moreover, because of the achiral and low-loss properties of the silicon dimers, small background absorption is present and thus the dissymmetry factor favored in enantioselectivity is not sacrificed as in plasmonic nanostructures. Further improvements on performance are expected by properly arranging the dimers into a 2D array, where the collective excitation of the dimers can lead to a higher quality factor and stronger local fields.[35] Other materials that have a high refractive index and low loss at shorter wavelengths, such as titanium dioxide, can be employed for similar devices operating in the ultraviolet region.[36,37] Constructing Fano-like resonances from larger particle ensembles may enable enhanced CD and spectral shifts simultaneously,[4,12,38] leading to ultrasensitive detection of chiral molecules. Being able to generate and engineer chiral fields without employing complex architectures or lossy materials, we expect that our findings pave the way for the development of new platforms for CD spectroscopy, enantioselective sensing, sorting and photolysis.

## Conflicts of interest

There are no conflicts to declare.

## Acknowledgements

The authors acknowledge the financial support of National Science Foundation under grant number DMR-1654192.

## References

1. G. D. Fasman, *Circular Dichroism and the Conformational Analysis of Biomolecules*, Springer Science+Business Media, New York, 1996.
2. Y. Tang and A. E. Cohen, *Phys. Rev. Lett.*, 2010, **104**, 163901.
3. Y. Tang and A. E. Cohen, *Science*, 2011, **332**, 333-336.
4. E. Hendry, T. Carpy, J. Johnston, M. Popland, R. Mikhaylovskiy, A. Lapthorn, S. Kelly, L. Barron, N. Gadegaard and M. Kadodwala, *Nat. Nanotechnol.*, 2010, **5**, 783-787.
5. N. A. Abdulrahman, Z. Fan, T. Tonooka, S. M. Kelly, N. Gadegaard, E. Hendry, A. O. Govorov and M. Kadodwala, *Nano Lett.*, 2012, **12**, 977-983.
6. M. Schäferling, D. Dregely, M. Hentschel and H. Giessen, *Phys. Rev. X*, 2012, **2**, 031010.
7. T. Davis and E. Hendry, *Phys. Rev. B*, 2013, **87**, 085405.
8. X. Tian, Y. Fang and M. Sun, *Sci. Rep.*, 2015, **5**, 17534.
9. S. Lee, S. Yoo and Q.-H. Park, *ACS Photonics*, 2017, **4**, 2047-2052.
10. M. L. Nesterov, X. Yin, M. Schäferling, H. Giessen and T. Weiss, *ACS Photonics*, 2016, **3**, 578-583.
11. W. Zhang, T. Wu, R. Wang and X. Zhang, *J. Phys. Chem. C*, 2016, **121**, 666-675.
12. S. Zu, Y. Bao and Z. Fang, *Nanoscale*, 2016, **8**, 3900-3905.
13. A. García-Etxarri and J. A. Dionne, *Phys. Rev. B*, 2013, **87**, 235409.
14. C.-S. Ho, A. Garcia-Etxarri, Y. Zhao and J. Dionne, *ACS Photonics*, 2017, **4**, 197-203.
15. S. Yoo and Q.-H. Park, *Phys. Rev. Lett.*, 2015, **114**, 203003.
16. Y. Luo, C. Chi, M. Jiang, R. Li, S. Zu, Y. Li and Z. Fang, *Adv. Opt. Mater.*, 2017, **5**, 1700040.
17. R. M. Bakker, D. Permyakov, Y. F. Yu, D. Markovich, R. Paniagua-Domínguez, L. Gonzaga, A. Samusev, Y. Kivshar, B. Luk'yanchuk and A. I. Kuznetsov, *Nano Lett.*, 2015, **15**, 2137-2142.
18. D. M. Lipkin, *J. Math. Phys.*, 1964, **5**, 696-700.
19. L. D. Barron, *Molecular Light Scattering and Optical Activity*, Cambridge University Press, New York, 2004.
20. A. I. Kuznetsov, A. E. Miroshnichenko, M. L. Brongersma, Y. S. Kivshar and B. Luk'yanchuk, *Science*, 2016, **354**, aag2472.
21. J. van de Groep, T. Coenen, S. A. Mann and A. Polman, *Optica*, 2016, **3**, 93-99.
22. E. D. Palik, *Handbook of Optical Constants of Solids*, Academic Press, 1998.
23. M. Morita, T. Ohmi, E. Hasegawa, M. Kawakami and M. Ohwada, *J. Appl. Phys.*, 1990, **68**, 1272-1281.
24. I. V. Lindell, A. Sihvola, S. Tretyakov and A. Viitanen, *Electromagnetic Waves in Chiral and Bi-Isotropic Media*, Artech House, 1994.
25. A. O. Govorov and Z. Fan, *ChemPhysChem*, 2012, **13**, 2551-2560.
26. L. V. Besteiro, H. Zhang, J. Plain, G. Markovich, Z. Wang and A. O. Govorov, *Adv. Opt. Mater.*, 2017, **5**, 1700069.

27. G. Pescitelli and R. W. Woody, *J. Phys. Chem. B*, 2012, **116**, 6751-6763.
28. R. Henderson and P. N. T. Unwin, *Nature*, 1975, **257**, 28-32.
29. H. G. Khorana, G. E. Gerber, W. C. Herlihy, C. P. Gray, R. J. Anderegg, K. Nihei and K. Biemann, *Proc. Natl. Acad. Sci. U. S. A.*, 1979, **76**, 5046-5050.
30. H. Cang, Y. Liu, Y. Wang, X. Yin and X. Zhang, *Nano Lett.*, 2013, **13**, 5949-5953.
31. P. H. Camargo, M. Rycenga, L. Au and Y. Xia, *Angew. Chem. Int. Ed.*, 2009, **48**, 2180-2184.
32. B. L. Feringa and R. A. Van Delden, *Angew. Chem. Int. Ed.*, 1999, **38**, 3418-3438.
33. G. Balavoine, A. Moradpour and H. Kagan, *J. Am. Chem. Soc.*, 1974, **96**, 5152-5158.
34. V. V. Klimov, D. V. Guzatov and M. Ducloy, *Europhys. Lett.*, 2012, **97**, 47004.
35. C. Wu, N. Arju, G. Kelp, J. A. Fan, J. Dominguez, E. Gonzales, E. Tutuc, I. Brener and G. Shvets, *Nat. Commun.*, 2014, **5**, 3892.
36. R. C. Devlin, M. Khorasaninejad, W. T. Chen, J. Oh and F. Capasso, *Proc. Natl. Acad. Sci. U. S. A.*, 2016, **113**, 10473-10478.
37. M. Khorasaninejad and F. Capasso, *Science*, 2017, **358**, eaam8100.
38. T. Han, S. Zu, Z. Li, M. Jiang, X. Zhu and Z. Fang, *Nano Lett.*, 2018, **18**, 567-572.

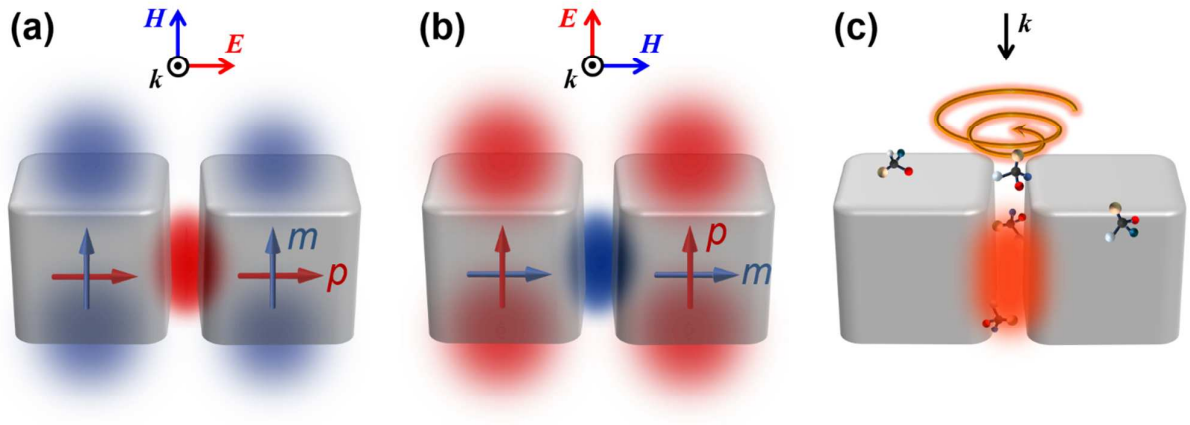


**Figure 1.** Schematic of hotspots generated in a high-refractive-index nanocube dimer. (a) An electric hotspot (blurring spot in red) occurs in the dimer gap when the electric field is polarized along the dimer axis to excite electric dipoles (*p*). (b) A magnetic hotspot (blurring spot in blue) takes place in the gap when the magnetic field is polarized along the dimer axis to excite magnetic dipoles (*m*). Red/blue arrows in the cubes indicate the direction of the induced electric/magnetic dipole moment. (c) A chiral hotspot (blurring spot in orange) arises in the dime gap upon illumination of circularly polarized light (CPL). Because the structure is achiral, the chirality of this hotspot always has the same sign as the incident CPL. When chiral molecules are adsorbed to the gap, strong chiral light-molecule interactions give rise to enhanced CD signals, while molecules at other locations have negligible contribution.

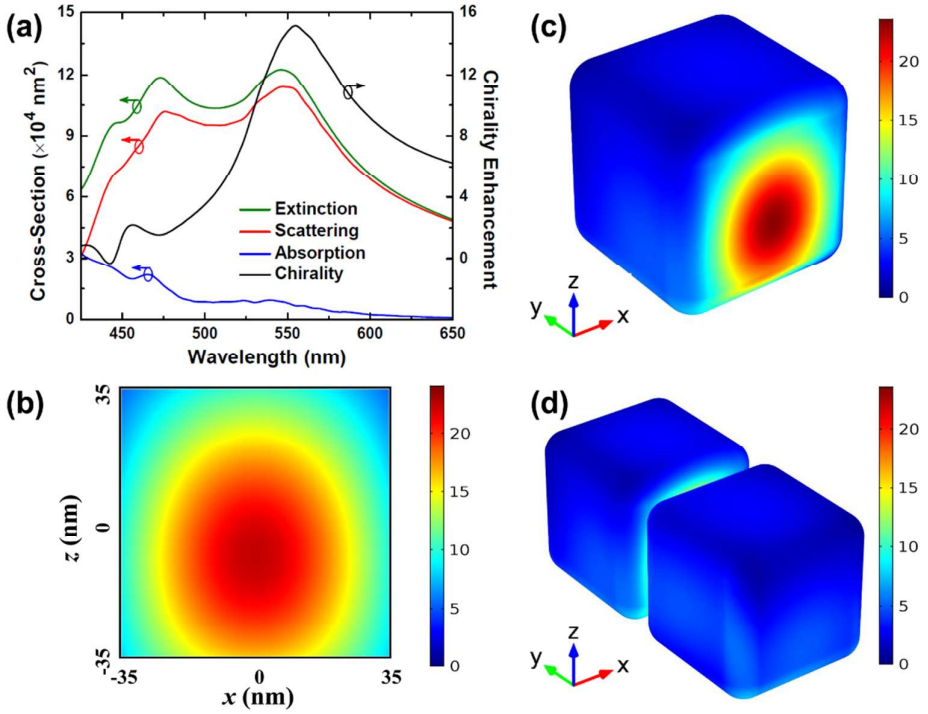


**Figure 2.** Enhanced optical chirality in a silicon nanocube dimer. (a) Spectrum of volume-averaged chirality in the dimer gap (black) and spectra of the scattering (red), absorption (blue), and extinction (green) cross sections of the dimer under top illumination of an RCP plane wave. (b) 2D map of optical chirality density on the cutting plane through the gap center at 555 nm wavelength. (c,d) Surface distribution of optical chirality observed from the gap (c) and from the end (d). Only one nanocube in the dimer is shown in (c) for clarity.

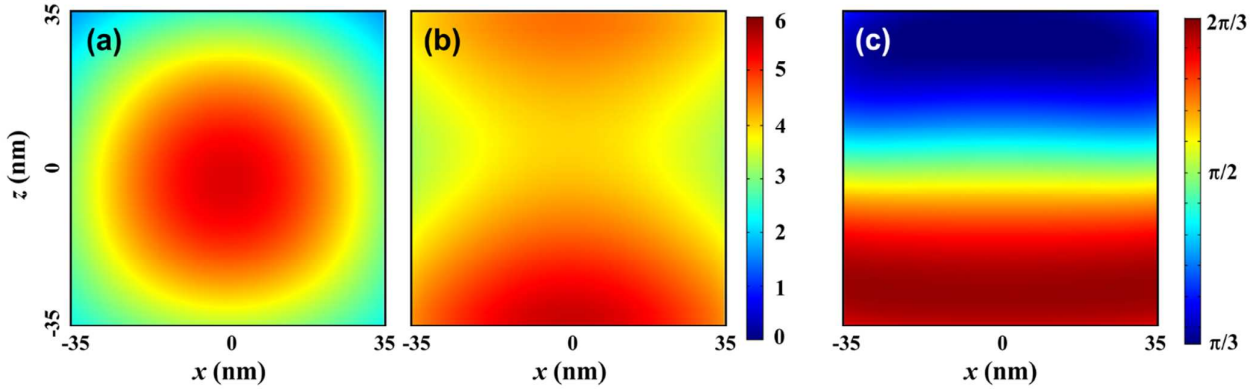


**Figure 3.** 2D maps of the magnetic (a) and electric (b) fields and their relative phase distribution (c) on the cutting plane through the dimer gap center. The field intensities show complementary patterns, which together with the relative phase close to π/2 satisfy all the conditions to maximize local optical chirality density.

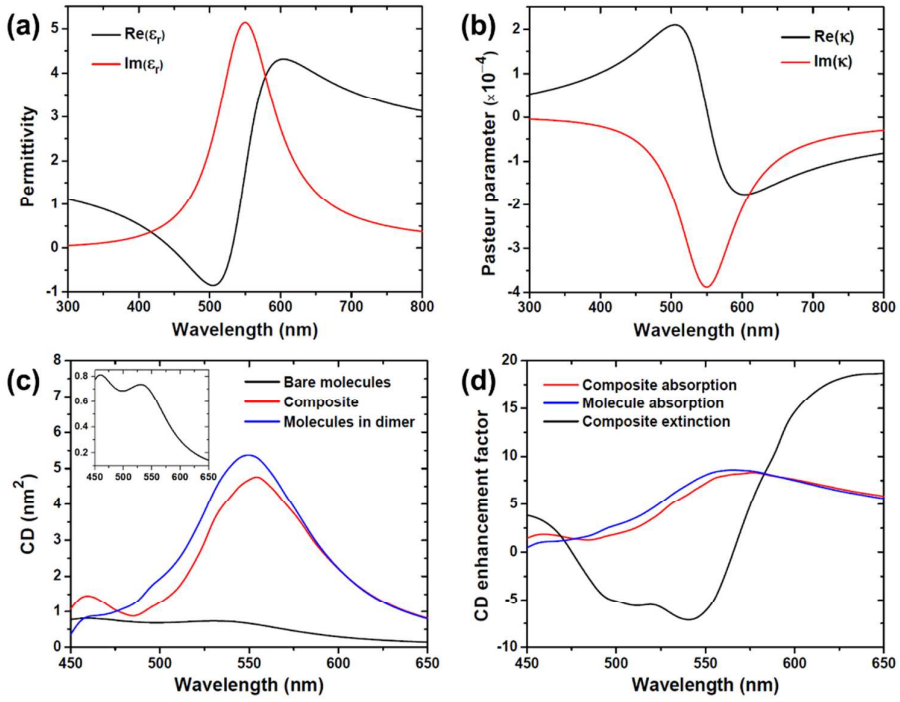


**Figure 4.** Dispersion of permittivity $\varepsilon_c$ (a) and the Pasteur parameter $\kappa$ (b) of the chiral molecules similar to bR. (c) The CD absorption spectra for chiral molecule with (red and blue curves) and without (black curve) the nanocube dimer. For the former, the CD signal is calculated in the whole composite (red) and in the chiral medium only (blue). Inset: Zoom-in image of the CD for bare molecules. (d) The CD enhancement factor.

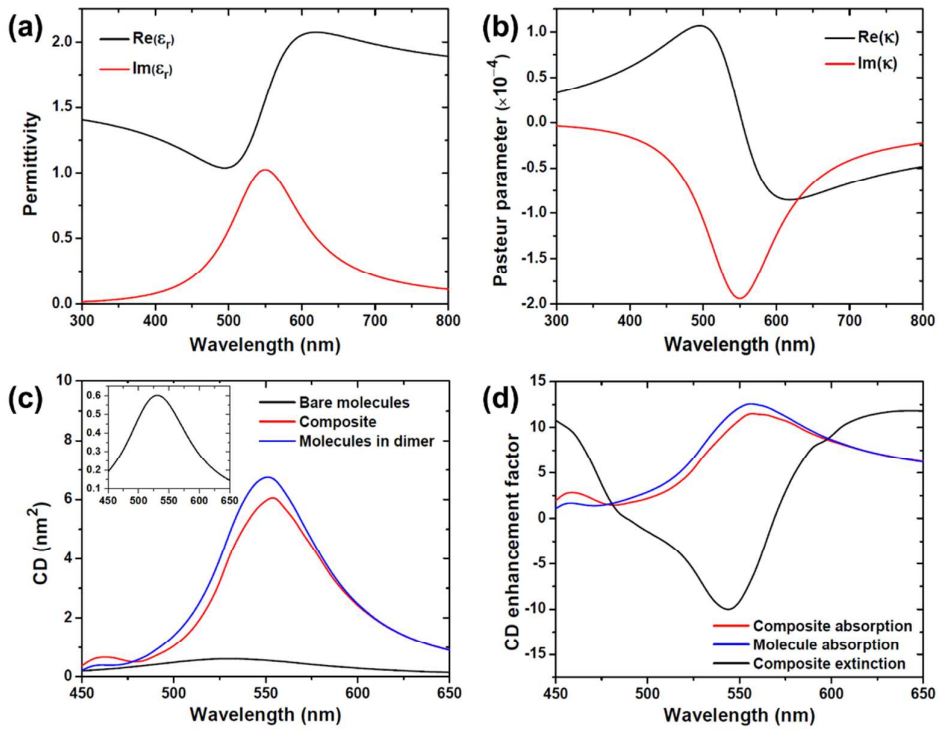


**Figure 5.** Dispersion of permittivity $\varepsilon_c$ (a) and the Pasteur parameter $\kappa$ (b) of the chiral molecules with typical extinction and CD values. (c) The CD absorption spectra for chiral molecule with (red and blue curves) and without (black curve) the nanocube dimer. For the former, the CD signal is calculated in the whole composite (red) and in the chiral medium only (blue). Inset: Zoom-in image of the CD for bare molecules. (d) The CD enhancement factor.

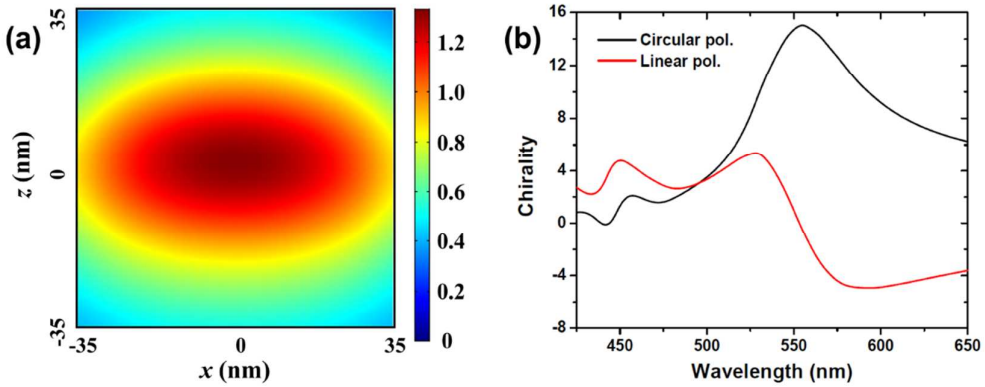


**Figure 6.** (a) Distribution of dissymmetry factor on the cutting plane through the gap center. (b) Comparison of volume-averaged chirality density in the dimer gap under the illumination of circularly (black) and linearly (red) polarized light.

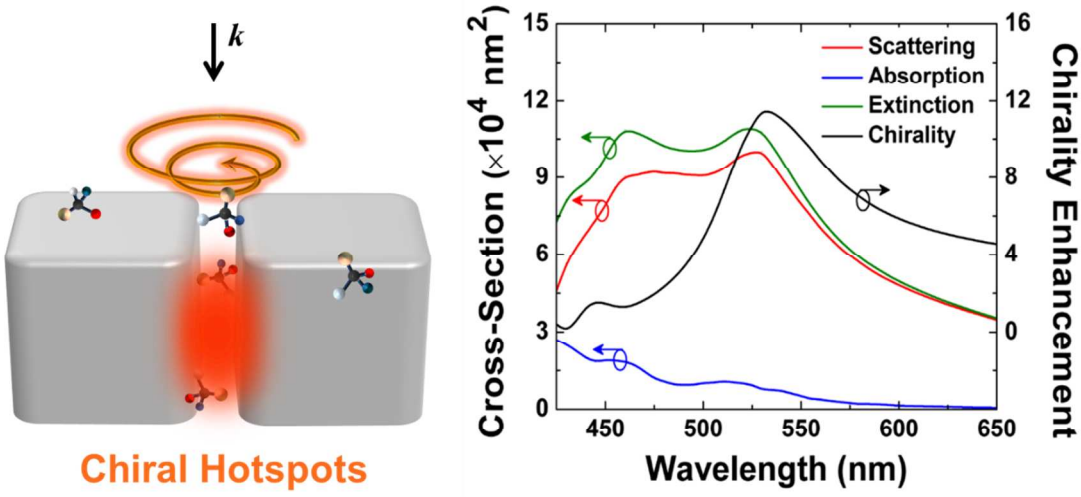


Chiral hotspots generated by achiral high-refractive-index dielectric nanoantennas can substantially enhance the CD signal without reducing the dissymmetry factor.